

This article was downloaded by:

On: 16 January 2011

Access details: *Access Details: Free Access*

Publisher *Taylor & Francis*

Informa Ltd Registered in England and Wales Registered Number: 1072954 Registered office: Mortimer House, 37-41 Mortimer Street, London W1T 3JH, UK



## Journal of Energetic Materials

Publication details, including instructions for authors and subscription information:

<http://www.informaworld.com/smpp/title~content=t713770432>

### Sensitivity of 2,6-Diamino-3,5-Dinitropyrazine-1-Oxide

Craig M. Tarver<sup>a</sup>; Paul A. Urtiew<sup>a</sup>; Tri D. Tran<sup>a</sup>

<sup>a</sup> Energetic Materials Center, Lawrence Livermore National Laboratory, Livermore, California, USA

**To cite this Article** Tarver, Craig M. , Urtiew, Paul A. and Tran, Tri D.(2005) 'Sensitivity of 2,6-Diamino-3,5-Dinitropyrazine-1-Oxide', Journal of Energetic Materials, 23: 3, 183 – 203

**To link to this Article:** DOI: 10.1080/07370650591001853

**URL:** <http://dx.doi.org/10.1080/07370650591001853>

PLEASE SCROLL DOWN FOR ARTICLE

Full terms and conditions of use: <http://www.informaworld.com/terms-and-conditions-of-access.pdf>

This article may be used for research, teaching and private study purposes. Any substantial or systematic reproduction, re-distribution, re-selling, loan or sub-licensing, systematic supply or distribution in any form to anyone is expressly forbidden.

The publisher does not give any warranty express or implied or make any representation that the contents will be complete or accurate or up to date. The accuracy of any instructions, formulae and drug doses should be independently verified with primary sources. The publisher shall not be liable for any loss, actions, claims, proceedings, demand or costs or damages whatsoever or howsoever caused arising directly or indirectly in connection with or arising out of the use of this material.

## Sensitivity of 2,6-Diamino-3,5-Dinitropyrazine-1-Oxide

CRAIG M. TARVER  
PAUL A. URTIEW  
TRI D. TRAN

Energetic Materials Center, Lawrence Livermore  
National Laboratory, Livermore, California, USA

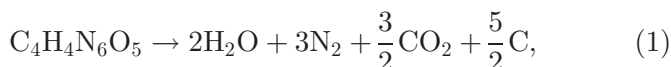
*The thermal and shock sensitivities of plastic bonded explosive formations based on 2,6-diamino-3,5-dinitropyrazine-1-oxide (commonly called LLM-105 for Lawrence Livermore Molecule #105) are reported. The One-Dimensional Time to Explosion (ODTX) apparatus was used to generate times to thermal explosion at various initial temperatures. A four-reaction chemical decomposition model was developed to calculate the time to thermal explosion versus inverse temperature curve. Three embedded man-ganin pressure gauge experiments were fired at different initial pressures to measure the pressure buildup and the distance required for transition to detonation. An Ignition and Growth reactive model was calibrated to this shock initiation data. LLM-105 exhibited thermal and shock sensitivities intermediate between those of triaminotri-nitrobenzene (TATB) and octahydro-1,3,5,7-tetranitro-1,3,5,7-tetrazine (HMX).*

**Keywords:** sensitivity, decomposition, thermal, LLM-105

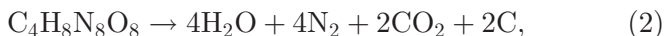
Address correspondence to C. M. Tarver, Energetic Materials Center, Lawrence Livermore National Laboratory, Livermore, CA 94551, USA. E-mail: tarver1@llnl.gov

## Introduction

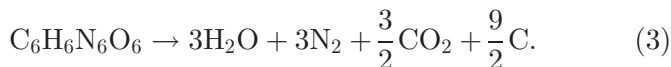
The explosive molecule 2,6-dinitro-3,5-dinitropyrazine-1-oxide was synthesized in the mid-1990s at Lawrence Livermore National Laboratory and designated LLM-105 for Lawrence Livermore Molecule #105. The synthesis route, scale-up procedures, and basic sensitivity properties of LLM-105 have been discussed by Pagoria [1]. LLM-105 has a high crystal density ( $1.913 \text{ g/cm}^3$ ) and an oxygen balance that suggests that it should be intermediate in sensitivity between triaminotrinitrobenzene (TATB) and octahydro-1,3,5,7-tetranitro-1,3,5,7-tetrazine (HMX). Its molecular formula and high-pressure, high-temperature reaction products are:



whereas HMX forms more  $\text{CO}_2$  and less solid carbon:



and TATB forms less  $\text{CO}_2$  and more solid carbon:



Small-scale testing by Cutting et al. [2] showed that LLM-105 is quite thermally stable and has an energy content of about 15% less than HMX and 20% more than TATB. Performance testing by Tran et al. [3] demonstrated that LLM-105 formulations can be readily initiated and deliver significant detonation energy in the modified Floret test [4]. The times to thermal explosion at various initial temperatures were measured in the One-Dimensional Time to Explosion (ODTX) apparatus [5] using the formulation RX-55-AA, which contains 95% LLM-105 and 5% Viton binder. In this paper a four-reaction chemical decomposition model for LLM-105 is developed and used together with a Viton decomposition model [5] to calculate ODTX explosion times for RX-55-AA. To determine the relative shock sensitivity of an LLM-105 formulation, three embedded manganin pressure gauge experiments were fired in a 100 mm diameter gas gun facility at different flyer plate impact velocities [6]. The LLM-105 formulation tested was

RX-55-AB, which contains 92.4% LLM-105 and 7.6% Kel-F binder. These experiments yielded time-resolved measurements of the pressure buildups behind the leading shock fronts at various distances into the explosive charges and the run distances to detonation at three input shock pressures, usually called “Pop Plot” data [7]. The experimental pressure histories were used to calibrate an Ignition and Growth hydrodynamic computer code reactive flow model [8] for the shock initiation and detonation of LLM-105. The thermal explosion experimental data and chemical kinetic decomposition model results are presented in the next two sections, followed by the experimental and calculated shock initiation results, and finally a Conclusions and Future Research section.

### Thermal Sensitivity of LLM-105

The ODTX apparatus [5] has been used to measure the times to explosion versus inverse temperature curves for many explosives. Spherical 1.27 cm diameter explosive charges are placed between preheated aluminum anvils, which are then rapidly closed and held together with a pressure of 0.15 GPa. The time required for the explosive decomposition to produce a sufficient quantity of gaseous reaction products to overcome the confinement pressure is accurately measured. Figure 1 shows the six ODTX times to explosion for RX-55-AA compared to those measured for LX-10 (95% HMX and 5% Viton) and LX-17 (92.5% TATB and 7.5% Kel-F binder). RX-55-AA exhibits a thermal sensitivity intermediate between the HMX and TATB formulations. The lowest temperature ODTX experiment at 463.55 K did not react in 86,400 sec (one day), so this temperature is below the critical temperature of RX-55-AA in this geometry. The violence of the RX-55-AA explosions in the ODTX apparatus is also intermediate between that of HMX-based explosives, whose increased cavity volumes after explosion were measured by Tarver and Tran [5], and that of TATB-based explosives, which produce relatively small increases in the spherical cavity volume upon explosion.

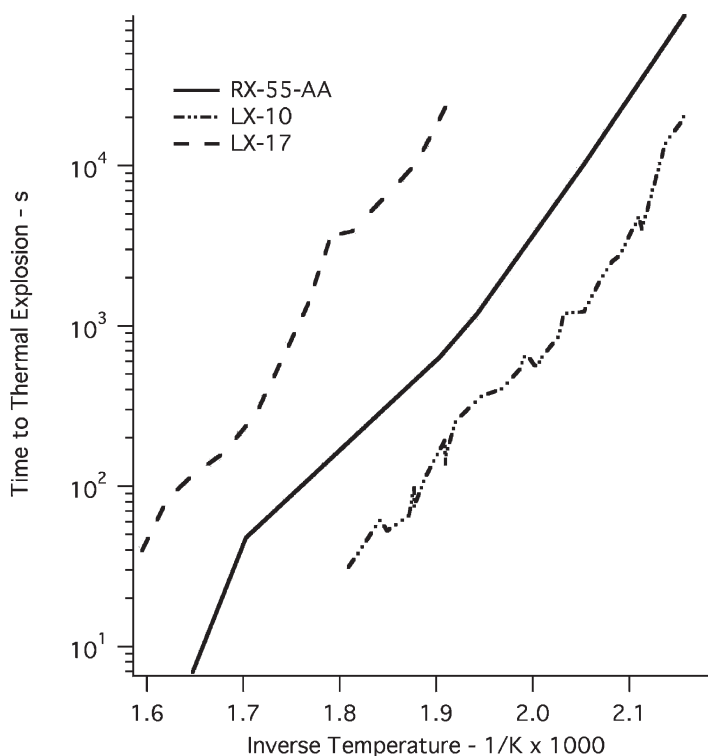
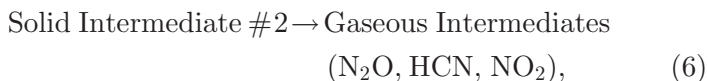


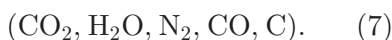
**Figure 1.** Experimental ODTX times to explosion for RX-55-AA, LX-17, and LX-10.

### Chemical Kinetic Decomposition Model for LLM-105

A four-step global chemical decomposition model has been developed for the thermal decomposition of LLM-105. This model consists of four reactions and five chemical species. This reaction sequence is the following:



GaseousIntermediates  $\rightarrow$  FinalProducts



The major pathways in HMX and TATB decompositions have been recently discussed by Tarver [9]. Little is currently known about LLM-105, but its structure and stability imply that it mostly likely undergoes several endothermic steps to break down its ring and hydrogen bonding in a manner similar to TATB. Reactions (4) and (5) are both assumed to be endothermic and produce smaller, less stable solid intermediates no. 1 and no. 2. Various solid intermediates can be postulated based on the bonds broken and the gases formed. Then reaction (6) represents a slightly exothermic formation of intermediate gaseous products, such as  $\text{N}_2\text{O}$ ,  $\text{HCN}$ ,  $\text{NO}_2$ , etc. Finally reaction (7) represents the gas phase formation of the final stable product gases  $\text{CO}_2$ ,  $\text{H}_2\text{O}$ ,  $\text{N}_2$ ,  $\text{CO}$ , etc., and solid carbon as the major portion of the total heat of reaction is released. The endothermic decomposition of the Viton binder in RX-55-AA is treated as a single reaction with the reaction rate constants given by Tarver and Tran [5].

Table 1 lists the thermal property and reaction rate parameters for the RX-55-AA decomposition model. The thermal conductivity of LLM-105 is assumed to be intermediate between those of TATB and HMX. LLM-105 has considerable hydrogen bonding, which implies a relatively high thermal conductivity. However, it is not as completely hydrogen bonded as the symmetrical TATB molecule, which has the highest thermal conductivity of the common organic explosive molecules. The initial bond-breaking reactions in HMX and TATB have average activation energies of 52.7 and 60 kcal/m, respectively [9], so the initial decomposition of LLM-105 in reaction (4) is assumed to have an intermediate value of approximately 57 kcal/m. The second endothermic step reaction (5) has a lower activation energy, which is assumed to be approximately 50 kcal/m in this model. The gas producing reactions (6) and (7) have activation energies of approximately 43 and 36 kcal/m, m, respectively. The heats of reaction are 50 cal/g endothermic for reactions (4) and (5), 200 cal/g exothermic for reaction (6),

**Table 1**  
Thermal and reaction rate parameters for RX-55-AA model

LLM-105	Solid intermediate #1	Solid intermediate #2	Intermediate gases	Final gases
1. Initial density = 1.88 g/cm <sup>3</sup>				
2. Heat capacity (cal/g-K) at:				
298 K	0.24	0.22	0.24	0.27
373	0.30	0.27	0.26	0.28
433	0.34	0.31	0.27	0.28
563	0.40	0.36	0.29	0.29
623	0.46	0.42	0.31	0.30
773	0.55	0.50	0.35	0.31
>1273	0.55	0.50	0.42	0.35
3. Thermal conductivity (cal/cm-g-K) at:				
298 K	$1.57 \times 10^{-3}$	$1.40 \times 10^{-3}$	$1.05 \times 10^{-3}$	$1.0 \times 10^{-4}$
373	$1.23 \times 10^{-3}$	$9.20 \times 10^{-4}$	$7.5 \times 10^{-4}$	$1.0 \times 10^{-4}$

433	$9.85 \times 10^{-4}$	$9.20 \times 10^{-4}$	$9.20 \times 10^{-4}$	$9.20 \times 10^{-4}$	$9.2 \times 10^{-4}$	$1.0 \times 10^{-4}$
563	$8.57 \times 10^{-4}$	$8.57 \times 10^{-4}$	$8.57 \times 10^{-4}$	$8.57 \times 10^{-4}$	$8.57 \times 10^{-4}$	$1.0 \times 10^{-4}$
623	$7.50 \times 10^{-4}$	$7.50 \times 10^{-4}$	$7.50 \times 10^{-4}$	$7.50 \times 10^{-4}$	$7.5 \times 10^{-4}$	$1.0 \times 10^{-4}$
773	$1.00 \times 10^{-4}$	$1.00 \times 10^{-4}$	$1.00 \times 10^{-4}$	$1.00 \times 10^{-4}$	$1.0 \times 10^{-4}$	$1.0 \times 10^{-4}$
>1273	$1.00 \times 10^{-4}$	$1.00 \times 10^{-4}$	$1.00 \times 10^{-4}$	$1.00 \times 10^{-4}$	$1.0 \times 10^{-4}$	$1.0 \times 10^{-4}$

4. Heat of formation (cal/g)  $-144.0$   $-94.0$   $-44.0$   $-244.0$   $-1144.0$

5. Reaction rate parameters  $\text{Na}^x q Z e^{-E/RT}$  (where  $N_a$  is mass fraction):

Reaction	$\ln Z$	$E$ (kcal/mol)	Reaction order $x$	Heat of reaction $q$ (cal/g)
1	51.0	56.64	1	+50.0
2	42.5	49.68	1	+50.0
3	34.5	42.73	1	-200.0
4	29.0	35.77	2	-900.0
6. Viton reaction rate parameters				
1	32.7	38.57	1	+1400.0



and 900 cal/g exothermic for reaction (7). This overall heat of reaction of 1000 cal/g is reasonable for a molecule with the oxygen balance of LLM-105 during thermal decomposition. The times to thermal explosion for the ODTX geometry are calculated using the Chemical TOPAZ heat transfer code [10]. Figure 2 shows the experimental and calculated times to thermal explosion for RX-55-AA at six values of inverse temperature. At the lowest temperature tested (463.55 K), no explosion was observed experimentally or computationally in 86,400 sec (24 hr). The agreement between the experimental and calculated times to explosion for RX-55-AA is reasonable. More time-to-explosion measurements and determination of

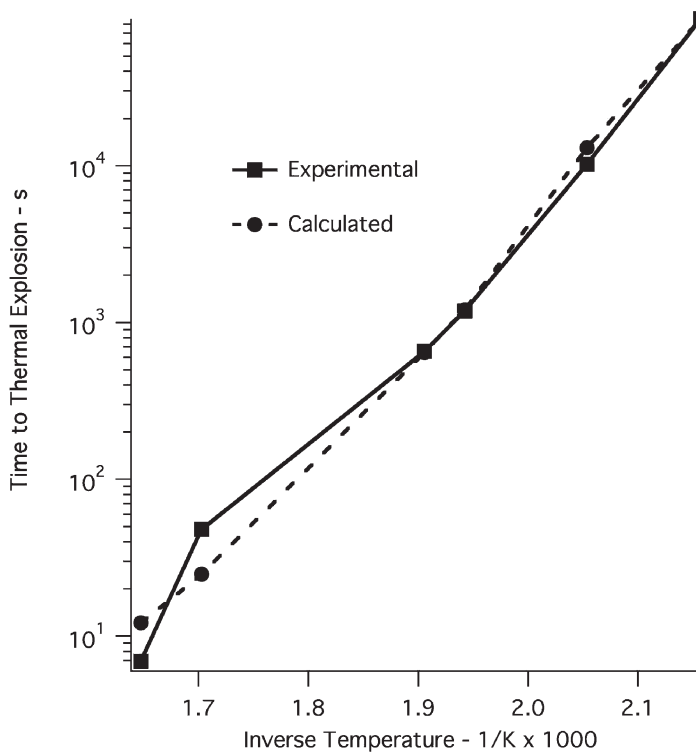


**Figure 2.** Experimental and calculated ODTX times to thermal explosion for RX-55-AA.

the thermal conductivity and heat capacity of LLM-105 as functions of temperature are needed to develop a more complete chemical decomposition model for LLM-105.

### Shock Initiation of LLM-105

The shock initiation of the LLM-105 formulation RX-55-AB (92.4% LLM-105 plus 7.6% Kel-F binder pressed to  $1.88 \text{ g/cm}^3$ , which represents 98% of its theoretical maximum density of  $1.92 \text{ g/cm}^3$ ) was determined using the 100 mm gas gun to accelerate aluminum discs into 3.4 cm long, 9 cm diameter cylindrical RX-55-AB targets containing embedded manganin pressure gauges along their axes. The three measured velocities for the 12.5 mm thick aluminum flyer plates were 0.729, 0.938, and 1.180 km/s, resulting in impact pressures of approximately 3.2, 4.2, and 5.4 GPa, respectively, in the RX-55-AB targets. A 3 mm thick aluminum buffer disc was placed in front of the first manganin gauge. The manganin gauges were placed depths of 0, 6.5, 13, and 19.5 mm into the RX-55-AB. Figures 3, 4, and 5 show the measured pressure histories for the three shock initiation experiments at impact velocities of 0.729, 0.938, and 1.180 km/s, respectively. Some of the manganin gauge records for the 3.2 GPa input pressure experiment in Figure 3 are noisy, but they clearly show that the shock-induced reaction in RX-55-AB increased the pressure to less than 9 GPa and did not cause detonation of this explosive charge within  $15 \mu\text{s}$ . At longer times, a two-dimensional reactive flow calculation showed that the rarefaction wave from the edge of the 4.5 cm radius LLM-105 charge has reached the center of the charge. This rarefaction wave causes gauge stretching and accompanying resistance increases that are not related to reaction-induced pressure increases [11]. At 3.2 GPa pressure, HMX-based plastic bonded explosives (PBXs) detonate after run distances of approximately 10 mm [12]. TATB-based PBXs do not react at all until shocked to over 6.5 GPa and exhibit pressure histories similar to those in Figure 3 at 8 GPa shock pressures [13]. At 4.2 GPa pressure in Figure 4, the manganin gauge records show that RX-55-AB transitions

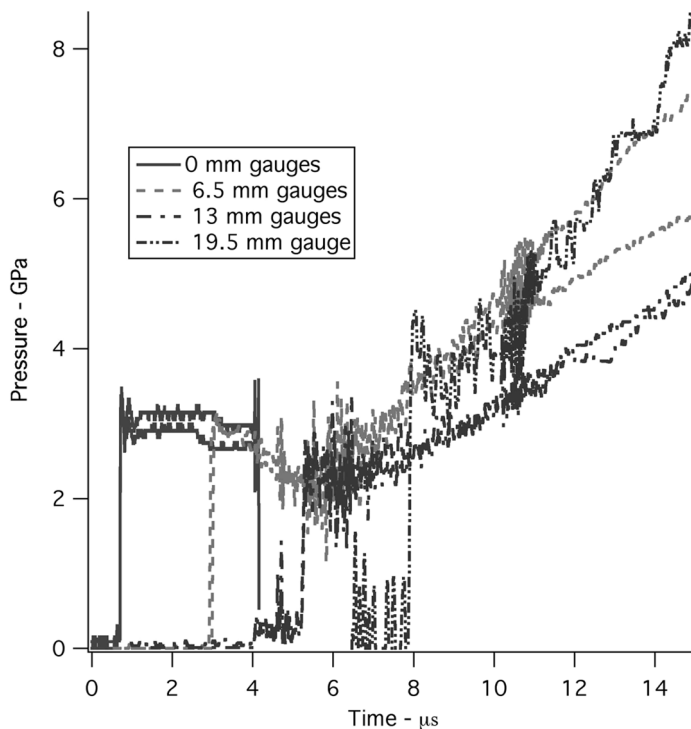


**Figure 3.** Experimental manganin pressure gauge records for LLM-105 impacted by aluminum flyer plate at 0.729 km/s.

to detonation just before the 13 mm deep gauge. At this shock pressure, HMX-based PBXs transition to detonation in 5–7 mm, and TATB-based PBXs do not react. At 5.4 GPa pressure in Figure 5, the RX-55-AB charge detonated near the 6.5 mm deep gauge. HMX-based PBXs detonate within 4–5 mm at 5.4 GPa, while TATB-based PBXs again fail to react at all. Therefore the LLM-105 based PBX RX-55-AB demonstrates a shock sensitivity intermediate between those of HMX and TATB-based PBXs.

The pressure histories at the gauges within the shock-induced reactive flow regions preceding detonation in Figures 3, 4, and 5 are typical of explosives of intermediate shock sensitivity, such as 2,4-dinitroimidazole (2,4-DNI) [14]. In such

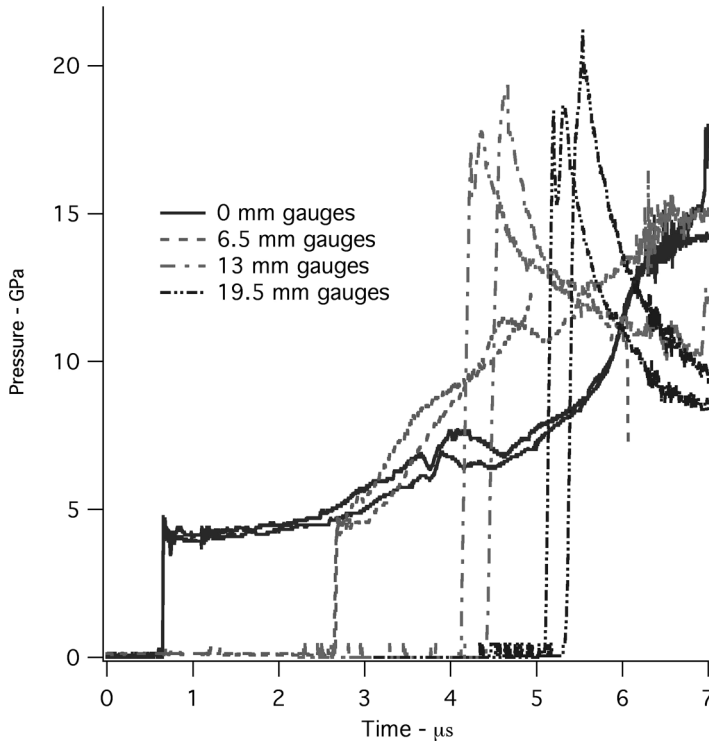


**Figure 4.** Experimental manganin pressure gauge records for LLM-105 impacted by aluminum flyer plate at 0.938 km/s.

explosives the pressure initially grows relatively slowly behind the lead shock, which does not increase rapidly in pressure as it propagates through the charge. The main growth of reaction occurs behind the leading shock, and transition to detonation occurs rapidly when the growing pressure pulse overtakes the leading shock.

### Initiation and Growth Shock Initiation Modeling of LLM-105

All reactive flow models require as a minimum two equations of state, one for the unreacted explosive and one for its reaction products; a reaction rate law for the conversion of explosive to products; and a mixture rule to calculate partially reacted

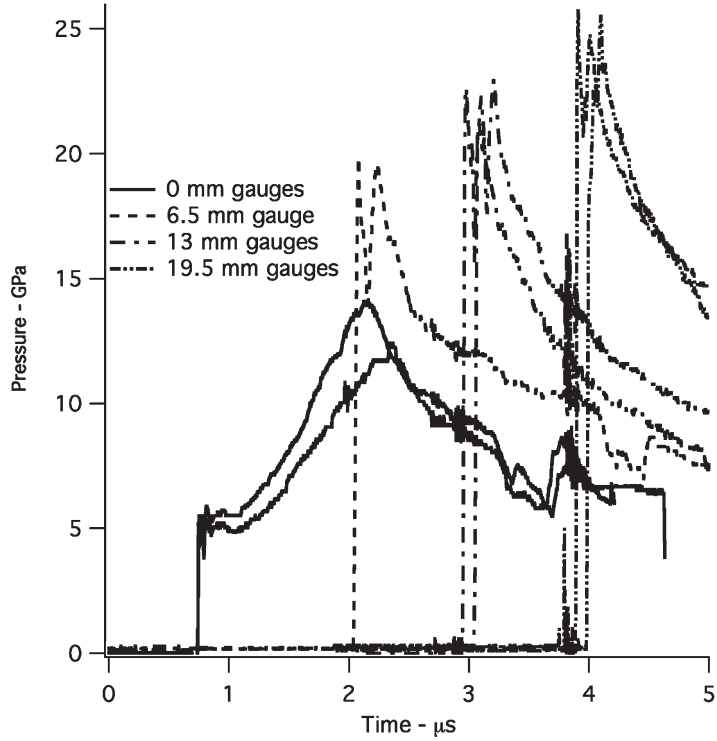


**Figure 5.** Experimental manganin pressure gauge records for LLM-105 impacted by aluminum flyer plate at 1.180 km/s.

states in which both explosive and products are present. The Ignition and Growth reactive flow model [8] uses two Jones-Wilkins-Lee (JWL) equations of state, one for the unreacted explosive and another one for the reaction products, in the temperature dependent form:

$$p = Ae^{-R_1 V} + Be^{-R_2 V} + \omega C_v T/V, \quad (8)$$

where  $p$  is pressure in Mbars,  $V$  is relative volume,  $T$  is temperature,  $\omega$  is the Grüneisen coefficient,  $C_v$  is the average heat capacity, and  $A$ ,  $B$ ,  $R_1$ , and  $R_2$  are constants. The unreacted explosive equation of state is fitted to the available shock Hugoniot data, and the reaction product equation of state is

fitted to cylinder test and other metal acceleration data. At the high pressures involved in shock initiation and detonation of solid and liquid explosives, the pressures of the two phases must be equilibrated, because interactions between the hot gases and the explosive molecules occur on nanosecond time scales. Various assumptions have been made about the temperatures in the explosive mixture, because heat transfer from the hot products to the cooler explosive is slower than the pressure equilibration process. In this version of the Ignition and Growth model, the temperatures of the unreacted explosive and its reaction products are equilibrated. Temperature equilibration is used, because heat transfer becomes increasingly efficient as the reacting "hot spots" grow and consume more explosive particles at the high pressures and temperatures associated with detonation.

Fine enough zoning must be used in all reactive flow calculations so that the results have converged to answers that do not change with even finer zoning. Generally this requires a resolution of at least 10 zones per mm in detonation calculations. Fifty zones per mm are used in this paper.

The Ignition and Growth reaction rate equation is given by

$$\begin{aligned}
 dF/dt = & I(1 - F)^b(\rho/\rho_0 - 1 - a)^x \\
 & + G_1(1 - F)^c F^d p^y + G_2(1 - F)^e F^g p^z \quad (9) \\
 0 < F < F_{ig\ max} \quad & 0 < F < F_{G1\ max} \quad F_{G2\ min} < F < 1,
 \end{aligned}$$

where  $F$  is the fraction reacted,  $t$  is time in  $\mu\text{sec}$ ,  $\rho$  is the current density in  $\text{g}/\text{cm}^3$ ,  $\rho_0$  is the initial density,  $p$  is pressure in Mbars, and  $I$ ,  $G_1$ ,  $G_2$ ,  $a$ ,  $b$ ,  $c$ ,  $d$ ,  $e$ ,  $g$ ,  $x$ ,  $y$ ,  $z$ ,  $F_{ig\ max}$ ,  $F_{G1\ max}$ , and  $F_{G2\ min}$  are constants. This three-term reaction rate law represents the three stages of reaction generally observed during shock initiation and detonation of pressed solid explosives [8]. The first stage of reaction is the formation and ignition of "hot spots" caused by various mechanical energy dissipation mechanisms as the initial shock or compression wave interacts with the unreacted explosive molecules. Generally the fraction of solid explosive heated during shock compression is approximately equal to the original void volume. The LLM-105 based

PBX RX-55-AB was pressed to 98% of its theoretical maximum density, so 2% of the explosive is assumed to be reacted by the first term in Equation (9). For shock initiation modeling, the second term in Equation (9) then describes the relatively slow process of the inward and/or outward growth of the isolated “hot spots” in a deflagration-type process. The third term represents the rapid completion of reaction as the “hot spots” coalesce at high pressures and temperatures, resulting in transition from shock-induced reaction to detonation [15].

For detonation modeling, the first term again reacts a quantity of explosive less than or equal to the void volume after the explosive is compressed to the unreacted von Neumann spike state. The second term in Equation (9) models the fast decomposition of the solid into stable reaction product gases ( $\text{CO}_2$ ,  $\text{H}_2\text{O}$ ,  $\text{N}_2$ ,  $\text{CO}$ , etc.). The third term describes the relatively slow diffusion-limited formation of solid carbon (amorphous, diamond, or graphite) as chemical and thermodynamic equilibrium at the C-J state is approached. These reaction zone stages have been observed experimentally using embedded gauges and laser interferometry to within several nanoseconds time resolution [16,17].

The Ignition and Growth reactive flow model has been applied to experimental shock initiation and detonation data using several one-, two-, and three-dimensional hydrodynamic codes. In shock initiation applications, it has successfully calculated embedded gauge, run distance to detonation, short pulse duration, multiple shock, reflected shock, ramp wave compression, and divergent flow experiments on several high explosives at various initial temperatures (heating plus shock scenarios), densities, and degrees of damage (impact plus shock scenarios) [6,8,12]. For detonation wave applications, the model has successfully calculated embedded gauge, laser interferometric metal acceleration, failure diameter, corner turning, converging, diverging, and overdriven experiments [16–18].

The RX-55-AB Ignition and Growth model parameters used in these calculations are listed in Table 2. Since no unreacted shock Hugoniot data are available, the unreacted equation of state of RX-55-AB was estimated from the initial

**Table 2**  
 Ignition and growth parameters for RX-55-AB,  
 $\rho_o = 1.88 \text{ g/cm}^3$

Unreacted JWL	Product JWL	Reaction rates
$A = 778.1 \text{ Mbar}$	$A = 7.1962 \text{ Mbar}$	$I = 1.24 \times 10^6 \mu\text{s}^{-1}$
$B = -0.05031 \text{ Mbar}$	$B = 0.13833 \text{ Mbar}$	$a = 0.11$
$R_1 = 11.3$	$R_1 = 4.5$	$b = 0.667$
$R_2 = 1.13$	$R_2 = 1.5$	$x = 7.0$
$\omega = 0.8938$	$\omega = 0.31$	$F_{ig\max} = 0.02$
$C_v = 2.487 \times 10^{-5} \text{ Mbar/K}$	$C_v = 1.0 \times 10^{-5} \text{ Mbar/K}$	$G_1 = 7.0 \text{ Mbar}^{-1} \mu\text{s}^{-1}$
$T_o = 298 \text{ K}$	$E_o = 0.0809 \text{ Mbar}$	$c = 0.667$
Shear modulus = 0.0354 Mbar		$d = 0.667$
Yield strength = 0.002 Mbar		$y = 1.0$
		$F_{G1\max} = 0.5$
		$G_2 = 2080 \text{ Mbar}^{-3} \mu\text{s}^{-1}$
		$e = 0.667$
		$g = 0.667$
		$z = 3.0$
		$F_{G2\min} = 0.0$

pressures measured by the three aluminum–RX-55-AB interface gauges in Figures 3–5 using the impedance matching technique [11]. A linear shock velocity  $U_s$ –particle velocity  $u_p$  relationship given by  $U_s = 2.0 \text{ km/s} + 1.87 u_p$  fits the three initial pressures well. This fit is close to that previously obtained in LX-17 embedded manganin gauge experiments [6], so the JWL equation-of-state parameters for unreacted LX-17 are used for the RX-55-AB calculations in this paper. The JWL reaction products equation of state listed in Table 2 is a preliminary fit to copper cylinder test expansion data for a



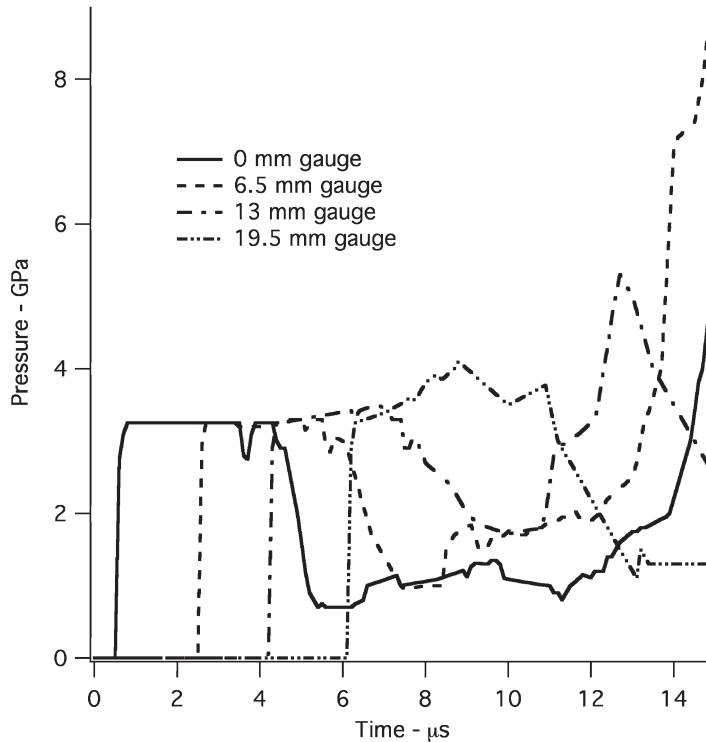


**Figure 6.** Calculated pressure histories for LLM-105 impacted by aluminum flyer plate at 0.729 km/s.

detonating LLM-105 PBX [19]. The reaction rate parameters in Table 2 use similar compression rate and pressure dependencies to those of LX-17, but are calibrated to the faster growth of reaction observed for RX-55-AB. Figures 6–8 show the calculated pressure histories at the embedded manganin gauges corresponding to the 3.2, 4.2, and 5.4 GPa experiments, respectively. The calculated pressure buildups at the gauges in the reactive flow preceding detonation, the arrival times of the shock waves at the gauge positions, and the run distances to detonation transition are all in good agreement with the experimental pressure histories shown in Figures 3–5. This Ignition and Growth model for RX-55-AB can be applied to other

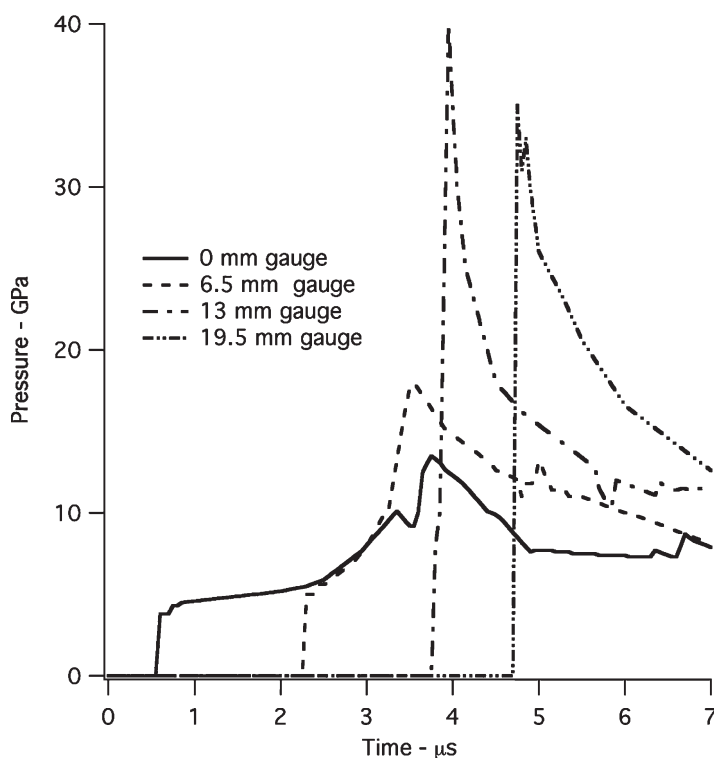


**Figure 7.** Calculated pressure histories for LLM-105 impacted by aluminum flyer plate at 0.938 km/s.

sustained shock scenarios with reasonable confidence. Additional shock initiation experiments using short time duration pulses, reflected shocks, and multiple shocks at various impact pressures are required to build a more complete Ignition and Growth reactive flow model for RX-55-AB.

## Conclusions and Future Research

This paper describes experimental thermal explosion and shock initiation data for LLM-105-based PBXs that show that this molecule is intermediate in thermal and shock sensitivity between HMX and TATB. The ODTX thermal explosion data

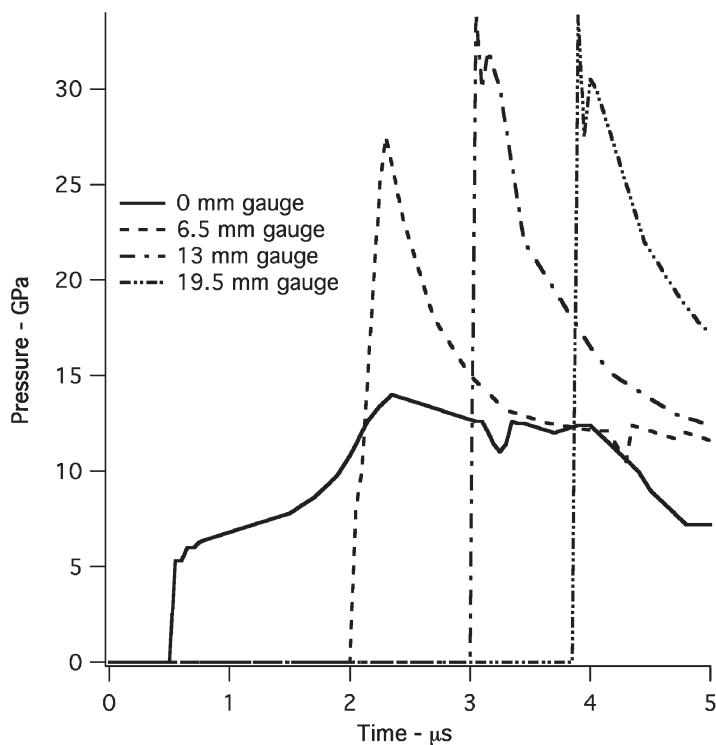


**Figure 8.** Calculated pressure histories for LLM-105 impacted by aluminum flyer plate at 1.180 km/s.

are used to develop a four-reaction chemical kinetic decomposition model for LLM-105, whose calculated times to explosion at various initial temperatures agree with the ODTX measurements. The embedded manganin pressure gauge technique is used to measure the shock initiation of the LLM-105 PBX RX-55-AB at three different initial pressures. An Ignition and Growth reactive flow model of the shock initiation and detonation transition of RX-55-AB is calibrated to this shock initiation data. The thermal decomposition kinetic model and the Ignition and Growth shock initiation model can be used to predict the time to explosion and run distance to detonation for other thermal and shock hazard scenarios, respectively.

However, these models can be considered only preliminary, because more experimental data are required to understand the sensitivity of LLM-105 PBXs as well as those based on HMX and TATB are understood. In the area of thermal explosion hazards, basic thermal properties, such as thermal conductivity and heat capacity, and chemical kinetic rates must be measured for LLM-105 as functions of temperature. Its PBXs must be tested in other thermal explosion experiments that quantitatively determine the violence of thermal explosion [20]. The deflagration rates of LLM-105 PBXs must be measured as functions of pressure and temperature [21]. More shock initiation experimental data on short-duration shock pulses, multiple shocks, reflected shocks, low-shock-pressure desensitization, and unreacted Hugoniot states are necessary for further refinement of the LLM-105 Ignition and Growth model before it is as reliable as the HMX and TATB models [22].

## Acknowledgments

The authors would like to thank Frank Garcia for building and firing the shock initiation experiments. This work was performed under the auspices of the United States Department of Energy by the Lawrence Livermore National Laboratory under Contract no. W-7405-ENG-48.

## References

- [1] Pagoria, P. F. 2005. Synthesis and scale-up of 2,6-diamino-3,5-dinitropyrazine-1-oxide (LLM-105), manuscript submitted for publication to *Propellants, Explosives, Pyrotechnics*.
- [2] Cutting, J. L., H. H. Chau, R. I. Hodgins, D. M. Hoffman, F. Garcia, R. S. Lee, E. McGuire, et al. 1998. *Eleventh International Detonation Symposium*, Aspen, CO: Office of Naval Research ONR 33300-5, pp. 828–835.
- [3] Tran, T. D., P. F. Pagoria, D. M. Hoffman, B. Cunningham, R. L. Simpson, R. S. Lee, and J. L. Cutting. 2002. Small-scale safety and performance characterization of new plastic bonded explosives containing LLM-105. *Twelfth International Detonation Symposium*, San Diego: CA, in press.

- [4] Lee, K., J. Kennedy, L. Hill, T. Spontarelli, J. Stine, and G. Kerley. 1998. *Eleventh International Detonation Symposium*, Aspen, CO: Office of Naval Research ONR 33300-5, pp. 362–370.
- [5] Tarver, C. M. and T. D. Tran. 2004. *Combustion and Flame*, 137: 50–62.
- [6] Forbes, J. W., C. M. Tarver, P. A. Urtiew, and F. Garcia. 1998. *Eleventh International Detonation Symposium*, Aspen, CO: Office of Naval Research ONR 33300-5, pp. 145–152.
- [7] Ramsay, J. B. and A. Popolato. 1965. *Fourth Symposium (International) on Detonation*, White Oak, MD: Office of Naval Research ACR-126, pp. 233–238.
- [8] Tarver, C. M., J. O. Hallquist, and L. M. Erickson. 1985. *Eighth Symposium (International) on Detonation*, Albuquerque, NM: Naval Surface Weapons Center NSWC MP 86-194, pp. 951–961.
- [9] Tarver, C. M. 2004. *Journal of Energetic Materials*, 22: 93–107.
- [10] Nichols, A. L., III and K. W. Westerberg. 1993. *Numerical Heat Transfer, Part B*, 24: 489–499.
- [11] Urtiew, P. A., L. M. Erickson, B. Hayes, and N. L. Parker. 1986. *Combustion, Explosion, and Shock Waves*, 22: 597–614.
- [12] Urtiew, P. A., J. W. Forbes, C. M. Tarver, K. S. Vandersall, F. Garcia, D. W. Greenwood, P. C. Hsu, and J. L. Maienschein. 2003. *Shock Compression of Condensed Matter—2003*, ed. M. D. Furnish, Y. M. Gupta, and J. W. Forbes, New York: AIP Press, pp. 1053–1056.
- [13] Bahl, K., G. Bloom, L. Erickson, R. Lee, C. Tarver, W. Von Holle, and R. Weingart. 1985. *Eighth Symposium (International) on Detonation*, Albuquerque, NM: Naval Surface Weapons Center NSWC MP 86-194, pp. 1045–1056.
- [14] Urtiew, P. A., C. M. Tarver, and R. L. Simpson. 1995. Shock Compression of Condensed Matter—1995. In S. C. Schmidt and W. C. Tao, eds., New York: AIP Press, pp. 887–890.
- [15] Tarver, C. M. and A. L. Nichols, III. 1998. *Eleventh International Detonation Symposium*, Aspen, CO: Office of Naval Research ONR 33300-5, pp. 599–605.
- [16] Tarver, C. M., J. W. Kury, and R. D. Breithaupt. 1997. *Journal of Applied Physics*, 82: 3771–3782.
- [17] Kury, J. W., R. D. Breithaupt, and C. M. Tarver. 1999. *Shock Waves*, 9: 227–237.
- [18] Tarver, C. M. and E. S. McGuire. 2002. Reactive flow modeling of the interaction of TATB detonation waves with inert

- materials. *Twelfth International Detonation Symposium*, San Diego: CA, in press.
- [19] Souers, P. C. 2004. Private communication, Lawrence Livermore National Laboratory.
- [20] Maienschein, J. L., J. F. Wardell, R. K. Weese, B. J. Cunningham, and T. D. Tran. 2002. Understanding and predicting the thermal explosion violence of HMX-based and RDX-based explosives. *Twelfth International Detonation Symposium*, San Diego: CA, in press.
- [21] Maienschein, J. L., J. F. Wardell, M. R. DeHaven, and C. K. Black. 2004. *Propellants, Explosives, Pyrotechnics*, 29: 287–295.
- [22] Tarver, C. M. and S. K. Chidester. 2005. *Journal of Pressure Vessel Technology*, 127: 39–48.